Electrical and dielectric investigations of the conduction processes in KY_3F_{10} crystals

1998 J. Phys.: Condens. Matter 10 5161

(http://iopscience.iop.org/0953-8984/10/23/016)

J. Phys.: Condens. Matter **10** (1998) 5161–5170. Printed in the UK PII: S0953-8984(98)88374-4

Electrical and dielectric investigations of the conduction processes in KY_3F_{10} crystals

A P Ayala†, M A S Oliveira†, J-Y Gesland‡ and R L Moreira†

† Departamento de Física, ICEx, Universidade Federal de Minas Gerais, CP 702, 30123-970 Belo Horizonte (MG), Brazil

‡ Université du Maine—Cristallogenese, 72025 Le Mans Cédex 09, France

Received 13 October 1997, in final form 13 January 1998

Abstract. Dielectric constant and ac and dc electrical conductivity measurements have been performed in single crystals of the fluorite compound KY_3F_{10}, in the temperature range 100 to 770 K. The dielectric response shows both dipolar and charge carrier contributions. The electrical conductivity varied more than 11 orders of magnitude and showed the existence of two thermally activated processes, with activation energies of 1.71(1) eV and 1.17(1) eV, for the higher and lower temperature regions, respectively. The conduction mechanisms have been discussed in terms of the different conduction pathways for the fluorine vacancy motion in the crystal.

1. Introduction

Interest in KY_3F_{10} crystals arises since materials containing the Y^{3+} trivalent rare earth ion in a non-centrosymmetrical site are very suitable as hosts for build up solid state lasers [1–3]. This crystal presents the fluorite-type structure (MF_2) belonging to the cubic O_h^5 spatial group ($Fm3m$), with $a = 11.54$ Å and two structural units per primitive cell [4–6]. The ionic groups $[KY_3F_8]^{2+}$ and $[KY_3F_{12}]^{2-}$ alternate along the three crystallographic axes, forming the multiple face centred cell ($Z = 8$), characteristic of the fluorite structure (figure 1). In the $[KY_3F_8]^{2+}$ motif, the fluorine ions, represented by F^2, form a cube (like in CaF_2), while in the $[KY_3F_{12}]^{2-}$ motif the twelve F^1 ions form a cube-octahedral cluster. Some characteristic interatomic distances are: F^1–F^1 = 2.6879 Å, F^2–F^2 = 2.4949 Å, K–F^1 = 3.2033 Å and K–F^2 = 2.8363 Å. These values show that the KY_3F_{10} structure is very closely packed, the interatomic distances being approximately the sum of the ionic radii involved.

From the electrical point of view, fluorite structures show high electrical conductivities at high temperatures, so that they can be classified as solid electrolytes [7–10]. In general, the high conductivity values attained at elevated temperatures come from a diffuse (or Faraday) phase transition to a fast conducting phase. The conduction mechanism is due to the appearance of anion Frenkel defects in the structure, allowing easy vacancy mobility. While Faraday transition has not been observed in KY_3F_{10}, previous investigations concerning the fluorine ion mobility present some discrepancies and misinterpretations, as discussed below.

Toshmatov *et al* studied this crystal using NMR and ac electrical conductivity [7]. They observed two thermally activated processes, one of them by NMR (600 to 750 K) and the other by ac conductivity (600 to 1000 K). These processes presented migration enthalphies of 1.1 eV and 1.5 eV respectively. The authors associate them with different conduction

0953-8984/98/235161+10$19.50

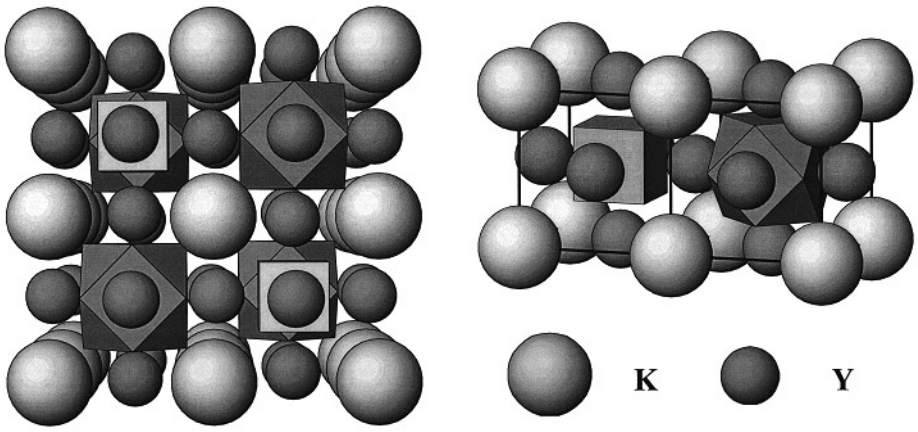

Figure 1. Crystalline structure of KY_3F_{10}. Unit cell (left) and structural motifs: $[KY_3F_8]^{2+}$ and $[KY_3F_{12}]^{2-}$ (right). The fluorine ions occupy the polyhedron vertices.

pathways in the crystal. Later, a Raman scattering investigation was accomplished by Mortier *et al* between 40 and 950 K [2]. The results presented in their work were consistent with the $Fm3m$ crystallographic structure of KY_3F_{10}, which showed it to be stable in all the temperature ranges investigated. As expected for ionic conductors, the Raman line widths increased at high temperatures. From this dependence Mortier *et al* obtained values for the activation energies ranging from 0.2 to 0.4 eV, which is of the same order of that expected for a Faraday conductor. Motivated by the important discrepancies between these results and by the lack of systematic studies on the electrical behaviour of KY_3F_{10}, we have performed a detailed experimental investigation of the ac and dc electrical conductivities of this material, between 100 and 770 K. The results presented in this work allow us to give a better picture on the conduction mechanism of this crystal.

2. Experimental procedures

Good quality KY_3F_{10} crystals were grown by the Czochralski technique. YF_3 was first synthesized by NH_4HF_2 fluorination of Y_2O_3 (5-nines grade, Shin-Etsu). Single crystals of KY_3F_{10} were pulled from a stoichiometric melt of $3YF_3 + KF$ (Suprapur grade, Merck), in a platinum crucible, along the [110] direction. The boules are easily cleaved along the {111} planes.

In view of the dielectric investigations, several plates were cut following the easy cleavage planes (typical surface area = 50 mm^2; thickness = 0.80 mm). Then, ac dielectric measurements were performed along the [111] direction, using an HP4192A impedance analyser in a parallel configuration (capacitance, conductance), as functions of frequency (10 Hz to 10 MHz) and temperature (100 to 770 K). The oscillation level was kept at 1.0 V rms. Silver paste electrodes were used to connect the samples to the holders in either a home made controlled furnace under nitrogen atmosphere or an evacuated Janis cryostat. The measurements were carried out either isothermally or under a continuous linear heating/cooling rates (2.0 K min^{-1}). Four-point dc conductivity (current measured with a Keithley 617 electrometer, for an applied voltage of 1.0 V and heating/cooling rates of 2.0 K min^{-1}) complements the data between 330 and 550 K.

3. Results

The temperature dependence of the real part of the dielectric constant (ε') of KY_3F_{10}, given in figure 2, shows a rather normal behaviour of an ordinary ionic crystal: ε' remains constant over a large temperature interval and becomes increasingly higher for higher temperatures. The latest effect is still more pronounced for lower frequencies. Indeed, the dielectric response has a contribution from the mobile ions, which leads to some sample polarization ($\varepsilon^*_{ionic} = \mathrm{j}\sigma^*(\omega)/\omega$, with $\sigma^*(\omega) \propto (\mathrm{j}\omega)''$, where $n \leqslant 1$, $\mathrm{j} = \sqrt{-1}$, ε^* is the complex dielectric permittivity and σ^* the complex electrical conductivity) [10, 11].

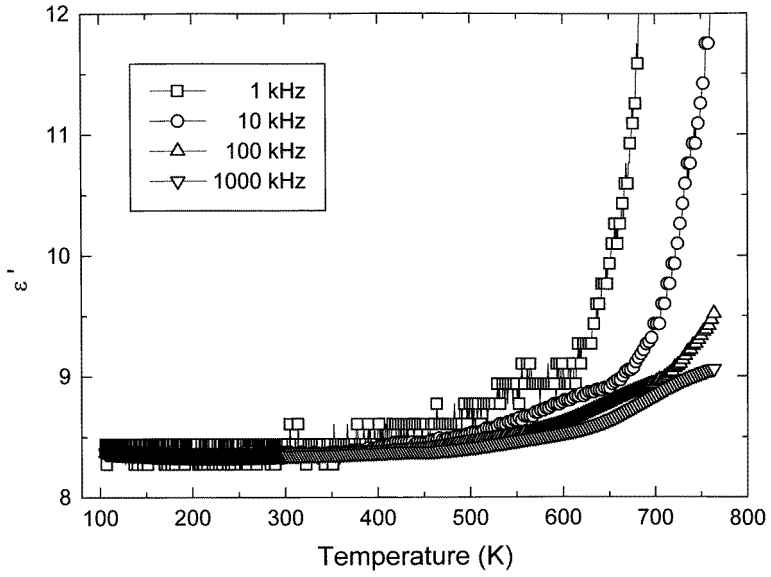

Figure 2. Temperature dependence of the dielectric constant of KY_3F_{10}, for some chosen measurement frequencies.

Let us now investigate the behaviour of the real part of the electrical conductivity $\sigma(\omega)$, versus temperature. As can be observed in figure 3, σ becomes increasingly frequency independent for higher temperatures, which can be interpreted as a consequence of the increasing jump frequency of the carriers [10] (the charges become increasingly free to move [12]). In addition, this figure indicates clearly the increasing of the electrical conductivity with temperature.

Since we have established the frequency independence of σ at higher temperatures, we can try to determine the activation energy of the conduction mechanism. Thus, we present in figure 4 a classical Arrhenius plot ($\log(\sigma T)$ against $1/T$) for the ac electrical conductivity data. The straight line representing the low frequency limit allows the determination of an intrinsic activation energy of 1.68(1) eV, for temperatures above 550 K. Note that, for increasing frequency, the separation of the measured conductivity from this 'static limit' line becomes larger. This is well compatible with the model outlined above for the jump conduction in solids [10]: for frequencies above the characteristic jump frequency, the charge carriers behave as dipole-like relaxators, bringing an additional (extrinsic) contribution to the measured conductivity.

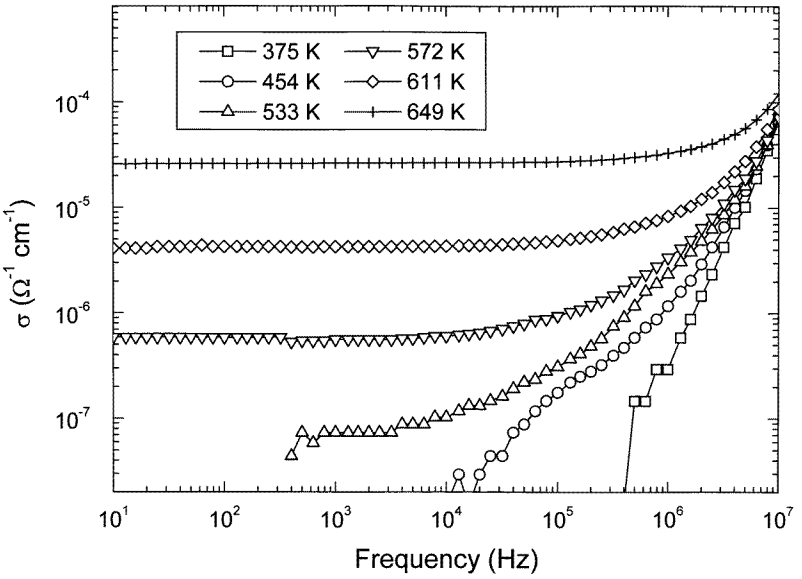

Figure 3. Frequency dependence of the electrical conductivity of KY_3F_{10}, for various temperatures, between 375 and 649 K.

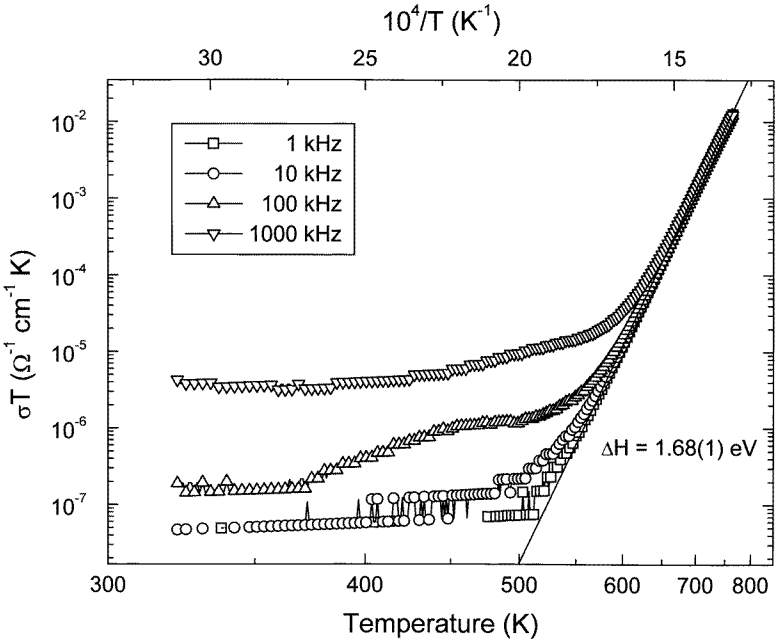

Figure 4. Arrhenius plot for the ac electrical conductivity of KY_3F_{10}, for the same frequencies as figure 2.

Since the intrinsic conductivity should be obtained for $\omega \rightarrow 0$, we used the classical Argand plot in order to verify the validity of the data treatment of figure 4. Our results are

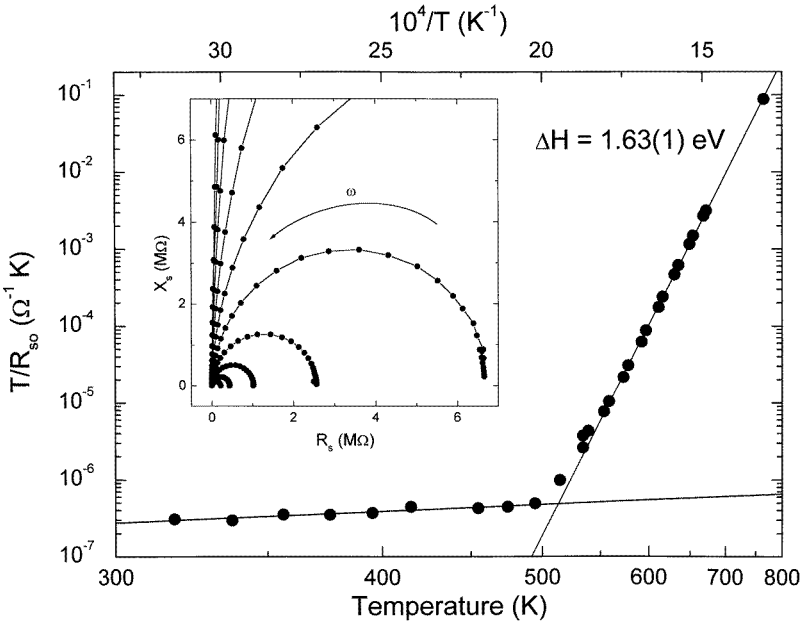

Figure 5. Arrhenius plot for the static series conductance (R_{s0}^{-1}) obtained from the Argand diagrams (X_s versus R_s) shown in the inset of the figure. The radii of the circles ($R_{s0}/2$) decrease with increasing temperature.

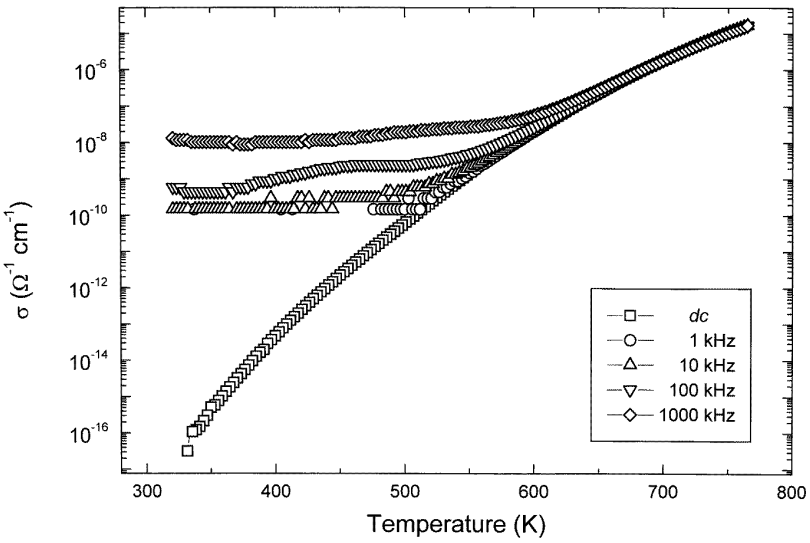

Figure 6. Comparison between ac and dc electrical conductivities, obtained for KY_3F_{10} crystal.

given in figure 5. In the inset of this figure we exemplify the Argand diagrams, where X_s and R_s are respectively the series reactance and resistance of the sample, calculated from the measured (parallel) ε' and σ. Note that the diagrams form complete semi-circles, with radii equal to $R_{s0}/2$, where R_{s0} is the static series resistance (equal to the inverse of the

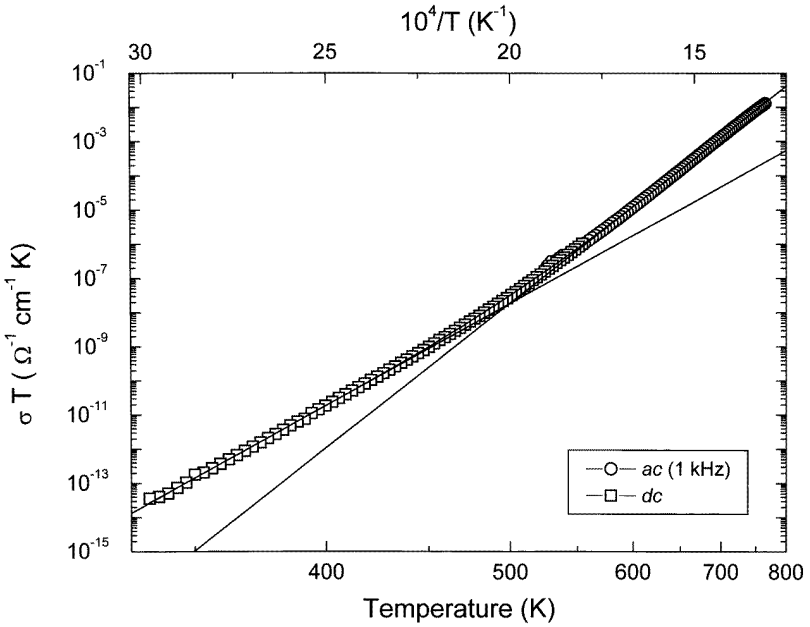

Figure 7. Arrhenius plot for the overall electrical conductivity of KY_3F_{10}, obtained from combined ac and dc data.

sample static series conductance). Thus, the plot of T/R_{s0} as a function of the reciprocal temperature should give the activation energy of conduction mechanism. As shown in figure 5, the obtained results are satisfactory for temperatures above 550 K, leading to an activation energy of 1.63(1) eV, roughly equivalent to that obtained on the previous treatment of $\log(\sigma T)$ against $1/T$. Nevertheless, the results below 550 K are affected by the measurement limit of the apparatus, i.e. the measured conductance becomes out of range. The straight line below 500 K corresponds to the saturation of the impedance analyser. The same behaviour is observed in figure 4, for the lowest frequency data.

The saturation of $\sigma(\omega, T)$ for low frequencies and temperatures occurs because the sample becomes highly resistive. Thus, this allows us to make dc electrical measurements without destroying the intrinsic properties of the sample (i.e., dry electrolysis is avoided). The results, obtained with the four-point method between 350 and 550 K, are presented in figure 6, in comparison with those obtained by the ac technique. We note that the curve for the static measurement matches very well the 'intrinsic' ac conductivity, i.e., the lowest frequency ac conductivity limit. Note that the combined data show 11 orders of magnitude of variation of the intrinsic conductivity, between 330 and 770 K.

We present now an overall analysis of the intrinsic electrical conductivity (figure 7). The temperature variation of σT above 330 K is well described by the sum of two thermally activated processes. Then a non-linear least squares fit was made using the following expression:

$$\ln(\sigma T) = A - \Delta H_1/kT + \ln[1 + B\exp(-(\Delta H_2 - \Delta H_1)/kT)]. \qquad (1)$$

In this way, the electrical conductivity appears to be characterized by (i) a higher temperature process, above 550 K, with a migration enthalpy (ΔH) 1.71(1) eV which is

slightly higher than the values obtained above; and (ii) a lower temperature process, with an activation energy of only 1.17(1) eV.

4. Discussion

The observation of two thermally activated conduction processes in KY_3F_{10} is well compatible with the existence of distinct paths for the vacancy movement in the crystal. In order to analyse the possible conduction paths it is convenient to consider separately the two structural units: $[KY_3F_8]^{2+}$ (RF_8) and $[KY_3F_{12}]^{2-}$ (RF_{12}). In the first one, the ions F^2 occupy the vertices of a cube, in a similar arrangement to CaF_2, while in RF_{12} the fluorine (F^1) form a cube-octahedron. As can be observed in figure 1, the yttrium atoms placed in the centre of the motif faces prevent conduction in the directions of the crystallographic axes. Then, we note that the movement of the fluorine vacancies cannot be along regular lattice sites, but rather through interstitial sites as in CaF_2. This determines that the conduction paths are in the [110] direction, through interstitial sites located in the edges of each motif. To explain the possible conduction mechanisms, only the interstitial site neighbourhood is redrawn in figure 8. These sites are in the middle of two concentric octahedra, one of them determined by four F^2 and two F^1; the other has a plane of four Y and two K. Based on this picture different possibilities for the vacancy ($V^{\cdot}_F$) filling can be proposed [7, 13]: (a) $F^x_{F^1} \leftrightarrow V^{\cdot}_{F^1}$; (b) $F^x_{F^2} \leftrightarrow V^{\cdot}_{F^2}$; (c) $F^x_{F^1} \leftrightarrow V^{\cdot}_{F^2}$; (d) $F^x_{F^2} \leftrightarrow V^{\cdot}_{F^1}$ (each possibility means the exchange between one kind of fluorine ion and one kind of fluorine vacancy). Toshmatov *et al* [7] suggested that the jumps (c) and (d) have the higher diffusion energies. Nevertheless, in their analysis of the more probable paths, they only consider the inner motif movements, which do not contribute to electrical conductivity, for which long-range motions are required. In fact, the macroscopic conduction process should be divided in two steps: inner motif movements and jumps between motifs (equivalent or not). In the isostructural $RbBi_3F_{10}$, Matar *et al* [13] determined that the inner motif movements require very low energies (0.17 eV). This allows us to conclude that the ionic conductivity in these crystals is dominated by the jumps between motifs. Following this reasoning and considering that the conduction pathways are through interstitial sites, we propose that only three thermally activated processes would produce net charge diffusion in these compounds, and thus would contribute to the electrical conductivity. These processes, whose detailed discussion is presented below, would be:

(i) $F^x_{F^1} \leftrightarrow V^{\cdot}_{F^1}$;
(ii) $F^x_{F^2} \leftrightarrow V^{\cdot}_{F^1}$ conjugated with $F^x_{F^1} \leftrightarrow V^{\cdot}_{F^2}$;
(iii) $F^x_{F^2} \leftrightarrow V^{\cdot}_{F^2}$.

Let us now discuss our model, which describes the main qualitative features of the ionic conductivity in KY_3F_{10}. Since this crystal presents two non-equivalent fluorine ions, the fluorine vacancy concentrations can be written as:

$$[V^{\cdot}_{F^j}][F'_i] = NN' z_j \, e^{-\beta G^f_j} \qquad [V^{\cdot}_F] = [V^{\cdot}_{F^1}] + [V^{\cdot}_{F^2}]$$
$$[V^{\cdot}_F][F'_i] = NN' \, e^{-\beta G^f_1}(z_1 + z_2 \, e^{-\beta(G^f_2 - G^f_1)}). \tag{2}$$

As usual, $\beta = (kT)^{-1}$, N and N' are the numbers of fluorine and interstitial sites respectively, $[V^{\cdot}_{F^j}]$ and $[F'_i]$ correspond to the numbers of F^j vacancies and interstitial fluorines F'_i, z_j is the fraction of F^j ions and G^f_j is the Frenkel pair formation energy. In a pure crystal, the charge neutrality requires that $[V^{\cdot}_F] = [F'_i]$. Thus, the ionic conductivity

would be given by:

$$\sigma(T) = \frac{4q^2}{kT}[\mathrm{F}_i']d_i^2\nu_i\,\mathrm{e}^{-\beta g'} + \sum_j \sigma_j(T) \tag{3}$$

where the first term describes the fluorine interstitial conduction and the summation corresponds to the three different processes for the $\mathrm{V}^{\cdot}_{F^1}$ and $\mathrm{V}^{\cdot}_{F^2}$ diffusion, as discussed above (σ_1: $\mathrm{F}^x_{F^1} \leftrightarrow \mathrm{V}^{\cdot}_{F^1}$; σ_2: $\mathrm{F}^x_{F^2} \leftrightarrow \mathrm{V}^{\cdot}_{F^1}$ coupled with $\mathrm{F}^x_{F^1} \leftrightarrow \mathrm{V}^{\cdot}_{F^2}$; and σ_3: $\mathrm{F}^x_{F^2} \leftrightarrow \mathrm{V}^{\cdot}_{F^2}$). Since the structure is closely compacted the simple interstitial fluorine diffusion ($\mathrm{F}'_i \leftrightarrow \mathrm{V}^x_i$) is not possible. Then, these ions could only diffuse by more complex processes such as an intersticialcy mechanism ($\mathrm{F}'_i \leftrightarrow \mathrm{F}^x_F \leftrightarrow \mathrm{V}^x_i$), but these processes are less probable and require more energy than vacancy diffusion. Thus, the first term of equation (3) can be neglected and the conductivity is entirely determined by vacancy diffusion, following the conduction pathways proposed above. The terms corresponding to the vacancy movement can be written as:

$$\begin{aligned}
\sigma_1(T) &= \frac{4q^2}{kT}[\mathrm{V}^{\cdot}_{F^1}]d_{11}^2\nu_1\,\mathrm{e}^{-\beta g_{11}} \\
\sigma_2(T) &= \frac{4q^2}{kT}2[\mathrm{V}^{\cdot}_{F^2}]d_{21}^2\nu_2\,\mathrm{e}^{-\beta g_{21}}\left(1 + 2\frac{[\mathrm{V}^{\cdot}_{F^1}]}{[\mathrm{V}^{\cdot}_{F^2}]}\frac{d_{12}^2}{d_{21}^2}\frac{\nu_1}{\nu_2}\,\mathrm{e}^{-\beta(g_{12}-g_{21})}\right) \\
\sigma_3(T) &= \frac{4q^2}{kT}2[\mathrm{V}^{\cdot}_{F^2}]d_{22}^2\nu_2\,\mathrm{e}^{-\beta g_{22}}
\end{aligned} \tag{4}$$

where d_{ij} and g_{ij} are the average displacements and migration energies for jumps between F^i and F^j sites and ν^j the F^j mobility.

In order to discuss the different conduction pathways we can benefit from previous data obtained with the NMR technique. The measurements of Toshmatov *et al* in this compound and the observations of Matar *et al* in the isostructural $RbBi_3F_{10}$, showed that the F^2 ions have higher internal mobility than the F^1 ones. This fact has a direct consequence in the electrical conductivity because even the $\mathrm{V}^{\cdot}_{F^1}$ vacancies, lying near the interstitial sites, are easily filled by F^2 ions and diffuse through RF_8 motifs better than through RF_{12}. Then, the processes (ii) and (iii) which involve the F^2 ions are more efficient than the process (i). The conduction in the process (ii) is determined by the σ_2 expression in (4) and some considerations can be made about this expression. From equation (2) the ratio between the numbers of fluorine vacancies is $[\mathrm{V}^{\cdot}_{F^1}]/[\mathrm{V}^{\cdot}_{F^2}] = z_1/z_2\,\mathrm{e}^{-\beta(G_1^f - G_2^f)}$. If the vacancy formation energies are approximately equal, this ratio will be approximately $z_1/z_2 \approx 3/2$. Furthermore, $d_{12}/d_{21} \approx 1$ and, since F^2 ions have higher mobility than F^1, the ratio ν_1/ν_2 is lower than one. Then, the term in parenthesis in the expression of σ_2 will be close to one and this contribution to the conductivity will have approximately a simple exponential behaviour characterized by the energy g_{21}. Therefore, the direct analysis of the expressions does not allow us to associate the different processes to the measured migration enthalpies (each case is characterized, or approximately characterized, by a simple exponential term).

Let us consider again figure 8, where the proposed conduction processes are indicated by arrows. Note that the simple process $\mathrm{F}^x_{F^2} \leftrightarrow \mathrm{V}^{\cdot}_{F^2}$ involves larger interatomic distances through the interstitial (F^2–F^2 = 5.2609 Å) than the $\mathrm{F}^x_{F^1} \leftrightarrow \mathrm{V}^{\cdot}_{F^1}$ exchange (F^1–F^1 = 2.7842 Å). We remark also that the three conduction pathways are all in the same average direction [110]. However, we notice that the fluorine octahedron is contracted in the direction that connects the F^1 ions (figure 8). In this way, the F^1 obstruct partially the diffusion path $\mathrm{F}^x_{F^2} \leftrightarrow \mathrm{V}^{\cdot}_{F^2}$, favouring the exchange $\mathrm{F}^x_{F^1} \leftrightarrow \mathrm{V}^{\cdot}_{F^2}$. Thus, process (iii) requires outward movements of the F^1, allowing the passage of the F^2 ions (this is viable because

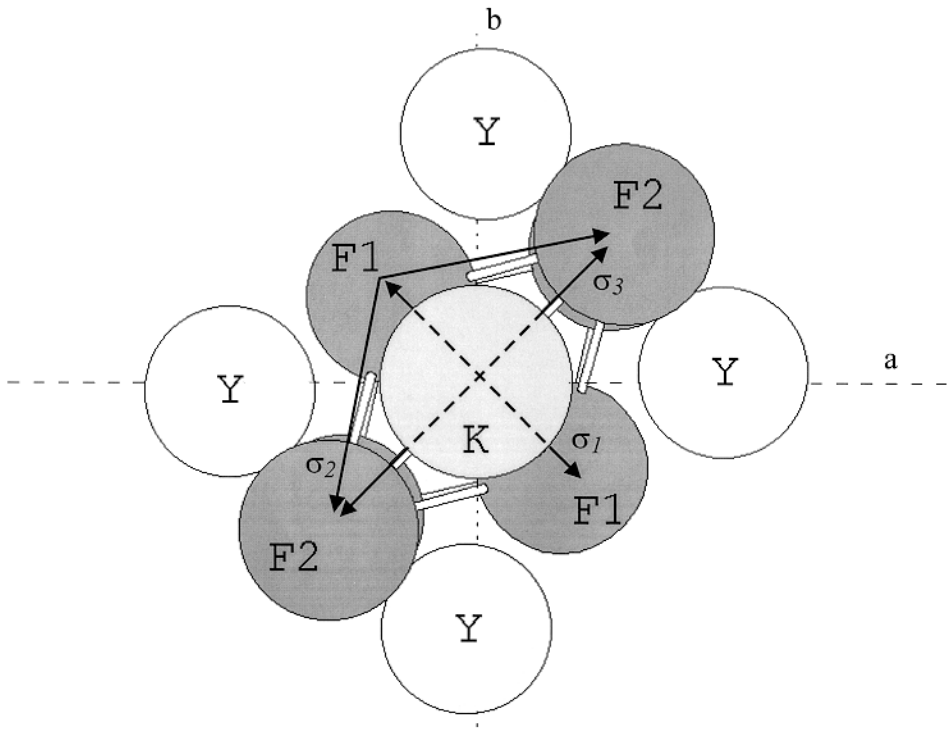

Figure 8. Atomic distribution in the interstitial site neighbourhood. The arrows correspond to the proposed conduction paths.

the RF_{12} cube-octahedron is less compact than the RF_8 cube). Therefore, two kinds of $V^{\cdot}_{F^2}$ diffusion can occur: in one of them the $F^x_{F^2} \leftrightarrow V^{\cdot}_{F^2}$ diffusion is assisted by the $F^x_{F^1} \leftrightarrow V^{\cdot}_{F^2}$ exchange (process (ii)), while in the other one, the F^1 participation is only by releasing space for the $F^x_{F^2} \leftrightarrow V^{\cdot}_{F^2}$ interchange (process (iii)). Thus, we suppose that the latest process involves higher diffusion energy than others since it requires an interstitial environment relaxation. If this assumption holds and considering that processes (ii) and (iii) are more efficient than (i), we propose that the measured high temperature process would be that of type (iii) (σ_3). For lower temperatures, when this process would become less efficient, the coupled migration (ii) (σ_2) would still permit vacancy migration through the RF_8 motifs. However, from our measurements, we cannot separate this mechanism from the process (i), because the small distance between the F^1 ions (for which there are no ions obstructing the exchange) could compensate its lower mobility. Therefore, at intermediate temperatures, the conduction would be through the more efficient process (ii) or by a mixed conduction between processes (i) and (ii). Finally, at still lower temperatures only the first process (i) would survive, since it corresponds to the pathway with the smallest interatomic distances. This situation could not be observed in our measurements, due to the high electrical resistance attained by the samples at low temperatures.

The observation of (at least) two conduction processes in KY_3F_{10} helps us to understand the discrepancies found by previous authors using different techniques: the conductivity values and activation energy of 1.5 eV found by Toshmatov *et al* [7], by electrical measurements above 600 K, are compatible with our higher energetic process. The same

authors found an activation energy of 1.1 eV below 600 K from the NMR line narrowing; this should correspond to our second measured process. Finally, Mortier *et al* [2] observed a very low activation energy (0.2 to 0.4 eV) through the line width broadening of some low frequency Raman bands. This effect was observed in a relatively wide temperature range (room temperature up to 950 K). This very low value can be reinterpreted considering that the vibrational modes are strictly perturbed by the vacancy movement within each motif. In fact, the energies observed by Mortier *et al* are compatible with the NMR results in $RiBi_3F_{10}$, where Matar *et al* obtained an energy of 0.17 eV, for the local movements of the fluorine vacancies.

5. Conclusion

Ac electrical conductivity measurements of KY_3F_{10} show: (i) a frequency dependent charge carrier contribution to the dielectric response at higher temperatures; (ii) a dipole-type relaxation (extrinsic) contribution to the electrical conductivity, mainly at lower temperatures and higher frequencies; (iii) an intrinsic ac contribution (higher temperatures, lower frequencies). The combination of the intrinsic ac conductivity data with the dc ones reveals the presence of two conduction processes, associated with the different pathways for the fluorine vacancy conduction in the crystal.

Acknowledgments

We thank Professor J F Sampaio for many helpful discussions and for a critical reading of the manuscript. This work has been partially supported by the Brazilian (CNPq, Finep and FAPEMIG) and French (CNRS) government agencies.

References

[1] Murray J R 1983 *IEEE J. Quantum Electron.* **QE-19** 488
[2] Mortier M, Gesland J-Y, Rousseau M, Pimenta M A, Ladeira L O, Machado da Silva J C and Barbosa G A 1991 *J. Raman Spectroscopy* **22** 393
[3] Debaud-Minorel A M, Mortier M, Buzaré J Y and Gesland J-Y 1995 *Solid State Commun.* **95** 167
[4] Pierce J W and Hong H Y P 1973 *Proc. 10th Conf. on Rare Earth Research (30 April–3 May 1973, Carefree, AZ)* vol 1, ed C J Kevane and T Moeller (Oak Ridge, TN: US Atomic Energy Commission) p 257
[5] Aleonard S, Le Fur Y, Pontonnier L, Gorius M F and Roux M Th 1978 *Ann. Chim. Fr.* **3** 417
[6] Mikou A 1986 *Thesis* Université de Limoges
[7] Toshmatov A D, Aukhadeev F L, Terpilovskiy D N, Dudkin V A, Zhdanov R Sh and Yagudin Sh I 1988 *Sov. Phys.–Solid State* **30** 61
[8] Beyeler H U, Bruesch P, Pietronero L, Schneider W R, Strassler S and Zeller H R 1979 *Physics of Superionic Conductors* ed M B Salamon (New York: Springer)
[9] Chandra S 1981 *Superionic Solids—Principles and Applications* (Amsterdam: North-Holland)
[10] Uvarov N F and Hairetdinov E F 1989 *Solid State Ion.* **36** 29
[11] Jonscher A K 1977 *Nature* **267** 673
[12] Belkaoumi M 1992 *Thesis* Université de Bourgogne, France
[13] Matar S, Reau J M, Villeneuve G, Soubeyroux J L and Hagenmuller P 1983 *Radiat. Eff.* **75** 55